European Journal of Nuclear Medicine and Molecular Imaging (2022) 49:2352–2363
https://doi.org/10.1007/s00259-022-05677-0

ORIGINAL ARTICLE

^{68}Ga-DOTATOC PET/MR imaging and radiomic parameters in predicting histopathological prognostic factors in patients with pancreatic neuroendocrine well-differentiated tumours

P. Mapelli[1,2] · C. Bezzi[1,2] · D. Palumbo[1,3] · C. Canevari[2] · S. Ghezzo[1,2] · A. M. Samanes Gajate[2] · B. Catalfamo[4] · A. Messina[1,3] · L. Presotto[2] · A. Guarnaccia[1] · V. Bettinardi[2] · F. Muffatti[5] · V. Andreasi[1,5] · M. Schiavo Lena[6] · L. Gianolli[2] · S. Partelli[1,5] · M. Falconi[1,5] · P. Scifo[2] · F. De Cobelli[1,3] · M. Picchio[1,2]

Received: 28 October 2021 / Accepted: 31 December 2021 / Published online: 14 February 2022

Abstract

Purpose To explore the role of fully hybrid ^{68}Ga-DOTATOC PET/MR imaging and radiomic parameters in predicting histopathological prognostic factors in patients with pancreatic neuroendocrine tumours (PanNETs) undergoing surgery.

Methods One hundred eighty-seven consecutive ^{68}Ga-DOTATOC PET/MRI scans (March 2018–June 2020) performed for gastroenteropancreatic neuroendocrine tumour were retrospectively evaluated; 16/187 patients met the eligibility criteria (^{68}Ga-DOTATOC PET/MRI for preoperative staging of PanNET and availability of histological data). PET/MR scans were qualitatively and quantitatively interpreted, and the following imaging parameters were derived: PET-derived SUVmax, SUVmean, somatostatin receptor density (SRD), total lesion somatostatin receptor density (TLSRD), and MRI-derived apparent diffusion coefficient (ADC), arterial and late enhancement, necrosis, cystic degeneration, and maximum diameter. Additionally, first-, second-, and higher-order radiomic parameters were extracted from both PET and MRI scans. Correlations with several PanNETs' histopathological prognostic factors were evaluated using Spearman's coefficient, while the area under the curve (AUC) of the receiver operating characteristic (ROC) curve was used to evaluate parameters' predictive performance.

Results Primary tumour was detected in all 16 patients (15/16 by ^{68}Ga-DOTATOC PET and 16/16 by MRI). SUVmax and SUVmean resulted good predictors of lymphnodal (LN) involvement (AUC of 0.850 and 0.783, respectively). Second-order radiomic parameters GrayLevelVariance and HighGrayLevelZoneEmphasis extracted from T2 MRI demonstrated significant correlations with LN involvement (adjusted $p = 0.009$), also showing good predictive performance (AUC = 0.992).

Conclusion This study demonstrates the role of the fully hybrid PET/MRI tool for the synergic function of imaging parameters extracted by the two modalities and highlights the potentiality of imaging and radiomic parameters in assessing histopathological features of PanNET aggressiveness.

Keywords Pancreatic neuroendocrine tumours · PET/MRI · Radiomics · ^{68}Ga-DOTA · Predictive value

This article is part of the Topical Collection on Oncology - General.

P. Mapelli and C. Bezzi contributed equally.

✉ M. Picchio
picchio.maria@hsr.it

[1] Vita-Salute San Raffaele University, Via Olgettina 58, 20132 Milan, Italy

[2] Nuclear Medicine Department, IRCCS San Raffaele Scientific Institute, Via Olgettina 60, 20132 Milan, Italy

[3] Department of Radiology, IRCCS San Raffaele Scientific Institute, Via Olgettina 60, 20132 Milan, Italy

[4] Department of Biomedical and Dental Sciences and of Morpho-Functional Imaging, Nuclear Medicine Unit, University of Messina, Piazza Pugliatti 1, 98125 Messina, Italy

[5] Pancreatic Surgery Unit, Pancreas Translational & Clinical Research Centre, IRCCS San Raffaele Scientific Institute, Via Olgettina 60, 20132 Milan, Italy

[6] Pathology Department, IRCCS San Raffaele Scientific Institute, Via Olgettina 60, 20132 Milan, Italy

Introduction

Neuroendocrine neoplasms (NENs) are rare and heterogeneous tumours with a large range of histological appearance, hormonal activity, molecular signature, and degree of aggressiveness [1].

Pancreatic neuroendocrine tumours (PanNETs) comprise only 1 to 2% of all pancreatic tumours, although a significant increase in incidence has been reported over the past few decades, especially due to an augmented awareness of physicians, along with improvements in high-quality imaging techniques [2].

Positron Emission Tomography (PET) imaging with ^{68}Ga-DOTA-conjugated peptides is the standard functional imaging modality to study well-differentiated PanNETs, being also included in the European guidelines [3]. Moreover, quantitative parameters derived from PET images, such as the maximum standardized uptake value (SUVmax), have demonstrated significant correlations with tumour characteristics and patients' prognosis [4–6].

Over the last few years, the combination of PET data with Computed Tomography (CT) or Magnetic Resonance Imaging (MRI) in integrated or hybrid imaging modalities has provided a great improvement in the detection of millimetric or even sub-millimetric lesions [7]; therefore, ^{68}Ga-DOTA peptide PET/CT or PET/MRI has become the imaging gold standard for NEN imaging. MRI provides higher soft tissue contrast compared to CT, along with functional imaging sequences including diffusion-weighted imaging (DWI). PET/MRI was thus recently shown to provide improved detectability of NEN lesions compared to PET/CT [8–11]. Moreover, it has been reported that ^{68}Ga-DOTATOC PET/MRI might be useful in predicting tumour grade and aggressiveness in NENs thanks to the simultaneous acquisition of morphological and functional MR sequences and PET images [12–14].

Radiomics represents a non-invasive emerging tool that is strongly implementing the characterization of tumour heterogeneity, with the ultimate goal of assisting the step toward personalized medicine. In the radiomic approach, quantitative information is extracted from medical images and analysed through specific algorithms, thus providing relevant sub-visual information on tissue pathophysiology, phenotype, and microenvironment [15].

The possibility to apply radiomics is still under debate, especially in the contexts of rare diseases such as PanNETs, being the lack of a methodological consensus among different studies one of the major weaknesses of this approach. A recent comprehensive review on the available literature on the methodological and technical approaches exploited in PanNET radiomic studies highlights the relevance of radiomics as a powerful tool able to improve diagnosis, surveillance, and treatment planning of PanNET patients, thus allowing non-invasive and cost-effective tailored management [16]. Moreover, the possibility to investigate several previously unexploited imaging data might be used to predict biological outcomes, thus suggesting the potentiality of the radiomic approach in the early stage and pre-operative characterization of PanNETs [16]. Several preliminary investigations explored the possible link between radiomic features and tumour characteristics of aggressiveness, as well as the predictive value of these quantitative parameters on treatment response [6, 17–20]. However, the currently available studies focused on NETs and molecular imaging includes small cohort of patients that are also inhomogeneous in terms of sites of origin (including NETs arising from different districts of the gastroenteropancreatic tract) and stage of disease (including patients undergoing ^{68}Ga-DOTA-peptide PET for staging, restaging, and treatment monitoring) [9, 21].

Moreover, the role of fully hybrid ^{68}Ga-DOTATOC PET/MRI-derived parameters in the field of PanNETs still remains barely unexplored, considering both imaging and radiomic parameters.

The aim of the present study was therefore to investigate the role of ^{68}Ga-DOTATOC PET/MR imaging and radiomic parameters of primary tumour in assessing histopathological prognostic factors in a homogeneous population of PanNET patients referred to surgery.

Methods

Patients

This retrospective study included patients with PanNET who underwent ^{68}Ga-DOTATOC PET/MRI scans for staging the disease.

Briefly, 187 consecutive ^{68}Ga-DOTATOC PET/MRI scans performed from March 2018 to June 2020 at IRCCS San Raffaele Scientific Institute in gastroenteropancreatic (GEP) NET patients were initially considered in this study and then selected according to the following inclusion criteria: (1) availability of simultaneous ^{68}Ga-DOTATOC PET/MR scan with a dedicated MRI study on the abdomen, (2) surgical intervention for primary PanNET and availability of histological data.

Exclusion criteria were: (1) simultaneous MRI acquired without contrast agent and performed only for anatomical coregistration of PET images, (2) PET/MRI study performed for reasons other than staging purpose, (3) primary NETs outside the pancreatic gland, and (4) no availability of histological data derived by surgical intervention for primary PanNET. Sixteen patients met the inclusion criteria and were then included in the study (Fig. 1). This relative low number

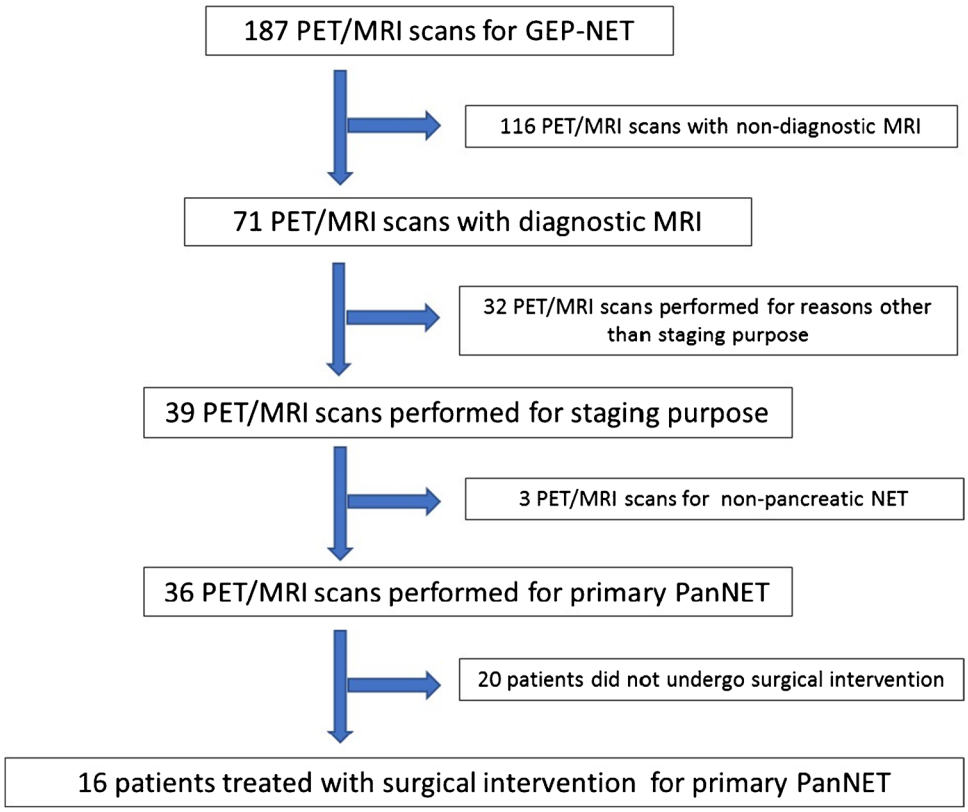

Fig. 1 Representation of participants' flow chart

of patients is coherent with the incidence of PanNETs and related to the retrospective design of the study and the rarity of PanNETs.

This study was approved by the Institutional Ethics Committee of IRCCS San Raffaele Scientific Institute, and all patients gave their informed consent to participate to the study.

PET/MRI acquisition protocol

Fasting condition was required on the day of the ^{68}Ga-DOTATOC PET/MRI scan. Images were acquired on a fully hybrid 3 Tesla PET/MRI system (SIGNA PET/MRI; General Electric Healthcare, Waukesha, WI, USA) in supine position, approximately 60 min after the injection of ^{68}Ga-DOTATOC (2.2–2.5 MBq/kg).

First, the patients underwent the total body PET/MR acquisition from the skull base to the knees (5/6 beds, each bed 4 min long) during which, the MR-based attenuation correction (MRAC) sequence, to be used for MR-based attenuation correction of PET data, the Lava Flex sequence, to be used for anatomical localization, and the DWI axial sequences have been acquired. The main reconstruction parameters of the Signa PET/MR scanner were as follows: 16 subsets, 3 iterations, Gaussian post filter FWHM 4 mm + TOF + PSF.

The total body scan was then followed by high-statistics (HS) PET/MR acquisition (10 min long) on the abdomen during which an axial T2 PROPELLER (periodically rotated overlapping parallel lines with enhanced reconstruction) Fat Sat, an axial DWI (*b* values: 50–200-700 s/mm^2), and a 2D WATS (dual echo with saturation of fat signal) sequence have been acquired simultaneously to the PET images. After that, an MR-only scan has been acquired consisting of the following: an axial 2D SPGR dual echo, a 3D Ideal for Fat Fraction calculation, a 3D Lava Flex Multiphase with hepato-specific (Primovist, Bayer Healthcare) contrast agent injection (1 phase before injection, and 3 phases afterward). Then, during the waiting time (20 min) before the final acquisition of the late enhancement axial and coronal Lava Flex images, a coronal and an axial SSFSE sequences have been acquired.

^{68}Ga-DOTATOC PET/MRI qualitative and quantitative analyses and imaging parameter estimation

^{68}Ga-DOTATOC PET/MRI image read-out has been performed on the Advantage Workstation (AW, General Electric Healthcare, Waukesha, WI, USA), on which PET, MRI, and fused PET/MRI images could be visualized in axial, coronal, and sagittal planes. PET images were qualitatively (positive vs. negative) interpreted by an experienced nuclear medicine physician, with knowledge of all the available

patients' clinical and imaging information. Findings with ^{68}Ga-DOTATOC uptake higher than physiological biodistribution were considered positive. Moreover, for each scan, the pancreatic primary lesion has been contoured and used for the quantitative PET image analysis. Specifically, a volume of interest (VOI) defining the focal pathological uptake, corresponding to the primary tumour, was contoured on ^{68}Ga-DOTATOC transaxial PET images. The applied segmentation was 3D, using a thresholding-based model with a cut-off of 40% of the SUVmax. The following PET semiquantitative parameters have been assessed: SUVmax, mean standardized uptake value (SUVmean), somatostatin receptor density (SRD), and total lesion somatostatin receptor density (TLSRD) [5, 6].

An experienced radiologist reviewed all MR images, blind to PET images and aware of patients' clinical information. MR images were analysed in terms of qualitative and quantitative parameters. Regarding qualitative analysis, the predominant enhancement pattern (arterial vs. venous), eventual cystic and/or necrotic component, and pure axial measurement assessment were evaluated on the primary tumours. For quantitative analysis, systematic collection of apparent diffusion coefficient (ADC) mean values, calculated on ROIs defined on ADC maps, was performed for each scan, carefully avoiding any eventual cystic/necrotic component.

^{68}Ga-DOTATOC PET/MRI-derived radiomic feature extraction

For each patient, manual segmentation of the entire focal pathological ^{68}Ga-DOTATOC uptake corresponding to the primary tumour was performed slice by slice, using both the draw and paint tools available in the Editor module of the open-source software 3D Slicer, version 4.11.2. (https://www.slicer.org). In order to assess interobserver reliability, PET-derived VOIs were contoured in a blinded fashion by two expert nuclear medicine physicians on transaxial PET images for the 15/16 patients showing ^{68}Ga-DOTATOC uptake. Similarly, MRI-derived VOIs were contoured for all the 16 patients in a blinded fashion by two radiologists on both the axial pre-contrast Lava Flex T1-weighted and the axial T2-weighted PROPELLER MRI sequences. After readers' segmentation, DICE coefficient was measured for each pair of VOIs in order to evaluate readers' agreement [22]. In case of disagreement, a new VOI was contoured by both the readers together, in accordance.

Then, images were normalized, resampled using the b-spline interpolation method to $3 \times 3 \times 3$ for PET scans, $0.8203 \times 0.8203 \times 1.7$ for MRI T1 scans, and $0.7422 \times 0.7422 \times 4.5$ for MRI T2 scans, and discretized using a fixed bin-width approach to reduce the continuous scales to 64 bins. Then, for each PET-, T1-, and T2-derived VOIs, radiomic features were extracted using the open-source Python package Pyradiomics 3.0.1 (https://www.radiomics.io/pyradiomics.html). Particularly, first-order, shape, gray level co-occurrence matrix (GLCM), gray level run length matrix (GLRLM), gray level size zone matrix (GLSZM), gray level dependence matrix (GLDM), and neighboring gray tone difference matrix (NGTDM) radiomic feature classes were extracted from both original and filtered images, the latter including wavelet and Laplacian of Gaussian (LoG) filtering. Overall, a total of 958 2D and 3D radiomic features of first-, second-, and higher-order were extracted from the primary tumours, for each of the three considered imaging modalities.

Surgery

Surgical resection was planned according to the site of the tumour and its dimension, and it has been performed according to previously published criteria [5, 6]. In particular, atypical resections, including middle pancreatectomy and enucleation, were performed in the presence of PanNETs less than or equal to 2 cm in size. PanNETs ≤ 2 cm with a strict relationship with the main pancreatic duct were excluded from enucleation. Typical resection included pancreaticoduodenectomy, distal pancreatectomy with or without splenectomy, and total pancreatectomy.

Pathology

Histological examination and immunostaining have been performed as previously described to diagnose PanNET and to determine the proliferative index (Ki67) and tumour grade on surgical specimens [5, 6]. The 2019 WHO classification was applied to determine tumour grade [23]. The Ki67 evaluation was expressed as a percentage based on the count of Ki67-positive cells within the tumour, using NCL-L-Ki67-MM1 (Novocastra, Newcastle Upon Tyne, UK) and KI67 CL. AQ530–9 (Ventana Medical Systems, Inc., Tucson, AZ, USA) antibodies; the spot with the highest immunostaining was considered when intratumoural heterogeneity was present. According to the European Neuroendocrine Tumor Society and UICC 2009, the relevant TNM stage was recorded for each tumour.

Statistical analysis

PET- and MRI-derived imaging parameters

The nonparametric Spearman's correlation coefficient was used to evaluate the correlation between ^{68}Ga-DOTATOC PET- and MRI-derived imaging parameters and tumours' histopathological prognostic factors, including grade, lymph node (LN) involvement, ratio between positive LNs

and overall number of resected LNs, and vascular invasion. Absolute values of the resulting correlations were interpreted as follows: 0.0–0.3 as negligible, 0.3–0.5 as low, 0.5–0.7 as moderate, 0.7–0.9 as high, and > 0.9 as very high. To avoid type I errors (false positives), adjustment for multiple comparisons was performed using the Benjamini-Hochberg's correction. P-values (*p)* lower than 0.05 were considered statistically significant.

Moreover, the receiver operating characteristic (ROC) curve analysis was performed to evaluate the ability of PET and MRI parameters in predicting the dichotomic histopathological prognostic factors of grade, LN involvement, and vascular invasion. The area under the curve (AUC), along with its 95% confidence interval (CI), was used to compare parameters' performance. Parameters showing an AUC significantly different from 0.5 (i.e., random condition) were considered informative, and interpreted in the following way: 0.7–0.8 as fair, and > 0.8 as good. For each parameter showing a statistically significant AUC, the optimal cut-off was derived by choosing the value corresponding to the point on the ROC curve nearest to the upper left corner of the ROC graph (standard method). All statistical analyses were performed using Python 3.7.

PET- and MRI-derived radiomic features

According to general guidelines [24], reliability of primary tumour manual segmentation was calculated by measuring the intraclass correlation coefficient (ICC) between the sets of features blindly extracted by the two nuclear medicine physicians/radiologists; ^{68}Ga-DOTATOC PET- and MRI-derived radiomics features with ICC values greater than 0.75 were selected for subsequent analyses. Data were standardized to a distribution with a mean value of 0 and a standard deviation value of 1. In order to reduce the number of features under investigation, highly correlated, redundant features were discarded by performing a correlation matrix evaluating the Pearson's correlation coefficient, and randomly retaining only one feature among those having a pairwise correlation higher than 0.80. As for the previously described imaging parameters, the nonparametric Spearman's correlation coefficient was used to evaluate the associations between the selected features and the histopathological prognostic factors of grade, LN involvement, and vascular invasion, while the ROC curve analysis was performed to evaluate radiomic features' predictive value.

Subsequent evaluations of statistically significant results included the Pearson's correlation coefficient measurements of association to check for potential redundancies among those features initially discarded by the correlation matrix, and the nonparametric Mann–Whitney *U* test to further describe features' ability in discriminating the different classes. All statistical analyses were performed using Python 3.7.

Results

Patients' population

Sixteen patients (9 males, 7 females; median age: 60 years, range: 41–76) were enrolled in the study.

According to the 2019 WHO classification, of these 16 patients, 10 patients had a G1 and 6 had a G2 PanNETs. The median Ki67 index was 2% (range: 1–10).

All patients had a non-functioning PanNET, 3/16 (18.7%) presented liver metastases at the time of diagnosis; at histological examination, 6/16 (37.5%) presented lymphnodal involvement, and 6/16 (37.5%) vascular invasion. Patients' characteristics are reported in Table 1.

^{68}Ga-DOTATOC PET/MRI findings

^{68}Ga-DOTATOC PET/MRI detected the primary tumour in all patients, with 1/16 not showing any ^{68}Ga-DOTATOC uptake in correspondence of the PanNET and being detected only by the MRI component; this patient presents a G1 NET lesion with Ki67 of 1% and maximum diameter of 40 mm at histological examination.

Median SUVmax, SUVmean, SRD, TLSRD, lesion diameter, and ADC, with correspondent ranges, are described in Table 1. Six of the 16 patients presented necrosis, 8/16 late enhancement, and 4/16 cystic degeneration (Table 1).

Among the 6 patients presenting lymphnodal involvement at histological examination, ^{68}Ga-DOTATOC PET/MRI identified only 1 patient having lymphnodal involvement, not showing any ^{68}Ga-DOTATOC uptake (Fig. 2); specifically, on MR images, a lymphnodal metastasis was identified in the right paracaval region (maximum diameter: 24 mm). Histological examination reported a pT3 pN1 G1 PanNET.

^{68}Ga-DOTATOC PET/MRI detected liver metastasis in 3/16 patients (19%); specifically, all 3/3 patients presented intense focal ^{68}Ga-DOTATOC uptake in correspondence of the pathological liver findings on diagnostic MR images. In Fig. 3, a representative case of a patient with liver metastases detected both on PET and MRI images is reported.

^{68}Ga-DOTATOC PET/MRI-derived imaging parameters

A significant, moderate, inverse correlation was observed between SUVmax and LN involvement (rho = −0.583, $p = 0.018$), as well as between SUVmax and the ratio between positive LNs and overall number of resected LNs (rho = −0.618, $p = 0.011$). Moreover, a low, inverse correlation approaching the level of significance was found between SUVmean and the ratio between positive LNs and overall number of resected LNs (rho = −0.493, $p = 0.052$)

Table 1 Patients' characteristics

Characteristic	Value	
Number of patients	16	
Male, ***n*** (%)	9 (56.3)	
Female, ***n*** (%)	7 (43.7)	
Median age, years (range)	60 (41–75)	
^{68}Ga-DOTATOC PET/MRI findings*	MRI	PET
Primary PanNET	16	15
Lymph nodes	1	0
Metastases (liver)	2	3
Pancreatic site, ***n*** (%)	6 (37.5)	
Head	1 (6.3)	
Isthmus	2 (12.5)	
Body	3 (18.7)	
Tail	4 (25)	
Body-tail		
Median lesion diameter, mm (range)	29.4 (8–76)	
Median Ki67, % (range)	2 (1–10)	
WHO 2017 classification, ***n*** (%)	10 (62.5)	
G1	6 (37.5)	
G2		
TNM		
T (*n*, %)		
T1	4 (25)	
T2	6 (37.5)	
T3	6 (37.5)	
N (*n*, %)		
N0	10 (62.5)	
N1	6[#] (37.5)	
M (*n*, %)		
M0	13 (81.3)	
M1	3 (18.7)	
^{68}Ga-DOTATOC PET parameters, median (range)		
SUVmax	70.67 (0–169.09)	
SUVmean	44.25 (0–111.15)	
SRD	4.99 (0–128)	
TLSRD	186.40 (0–3009)	
MRI parameters		
ADC, median (range)	0.95 (0.6–2)	
Necrosis, *n* (%)	6 (37.5)	
Late enhancement, *n* (%)	8 (50)	
Cystic degeneration, *n* (%)	4 (25)	

*Patient-based analysis; [#]1/6 perihepatic lymph node, 5/6 peripancreatic lymph nodes; *SUV*, standardized uptake value; *SRD*, somatostatin receptor density; *TLSRD*, total lesion somatostatin receptor density; *ADC*, apparent diffusion coefficient

and LN involvement (rho = −0.478, $p = 0.061$). However, after adjustment for multiple comparisons, observed p values lost the level of significance.

According to ROC analyses, both SUVmax and SUVmean resulted good predictors of LN involvement. Specifically, SUVmax showed an AUC of 0.850 (95% CI: 0.60–1.00), with an optimal cut-off value of 90.960 and correspondent sensitivity and specificity of 60% and 100%, respectively (Fig. 4a). Similarly, SUVmean showed an AUC of 0.783 (95% CI: 0.50–1.00), with an optimal cut-off value of 54.540 and correspondent sensitivity and specificity of 60% and 100% (Fig. 4b).

No significant correlation or predictive value was observed for the other PET-derived imaging parameters, nor for any of MR-derived parameters.

^{68}Ga-DOTATOC PET/MRI-derived radiomic features

After readers' segmentations of each imaging modalities, evaluation of the DICE coefficients allowed to detect few cases of disagreement, and in these cases, a new VOI was contoured by both the readers together, in accordance. After agreement was reached, DICE mean values for PET, T1, and T2 pairs of segmentations were 0.74, 0.81, and 0.81, respectively. At this point, 958 radiomic features were extracted from both the readers' segmentations for each imaging modalities, and ICC was calculated with initial mean value of 0.66 (range: 0.48–1.00) for PET features, 0.79 (range: 0.49–1.00) for T1 features, and 0.87 (range: 0.58–1.00) for T2 features. Radiomic features characterized by an ICC lower than 0.75 were discarded, and 457/958 PET features, 710/958 T1 features, and 822/958 T2 features were retained, with ICC values of the selected subsets ranging between 0.75 and 1.00 and with mean values of 0.91, 0.94, and 0.99, respectively.

Then, highly correlated, redundant features (Pearson's correlation coefficient > 0.80) were discarded, and a final set of 20 features for PET, 27 features for T1 sequence, and 42 features for T2 sequence were considered for subsequent analyses.

Different correlations between radiomic features and grade, LN involvement, and vascular invasion were identified, with an overall prevalence of LoG and original and wavelet features of 45.16%, 32.26%, and 22.58%, respectively. Generally, almost no overlap has been identified among the three considered imaging modalities between the features associated to the same histopathological prognostic factor. However, after adjustment for multiple comparisons, statistical significance held true exclusively for two original GLSZM texture features extracted from T2 MRI sequences. Specifically, original_glszm_GrayLevelVariance (GLV) and original_glszm_HighGrayLevelZoneEmphasis (HGLZE) both showed a significant, high, inverse correlation of −0.830 with LN involvement ($p < 0.005$, adjusted $p = 0.009$). The measured pairwise correlation value between the two features was 0.523 ($p = 0.038$), and no redundancy (rho ≥ 0.75) was found between each of the two features and

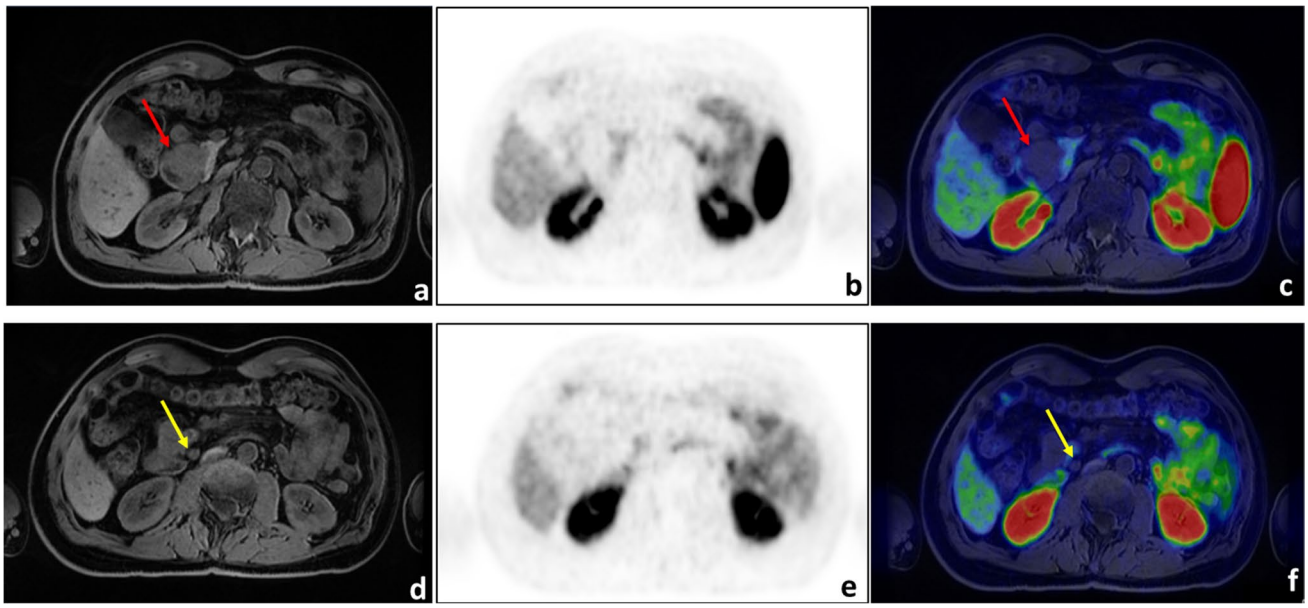

Fig. 2 ^{68}Ga-DOTATOC PET/MRI performed for PanNET staging. A 52-year-old patient underwent ^{68}Ga-DOTATOC PET/MRI. Axial Lava Flex MR images showed a lesion in the pancreatic head (**a**, red arrow), not showing any pathological uptake on ^{68}Ga-DOTATOC PET (**b**) and PET/MR (**c**, red arrow) images. A pathological right paracaval lymph node was also detected on axial Lava Flex MR images (**d**, yellow arrow), not presenting pathological uptake on ^{68}Ga-DOTATOC PET (**e**) and PET/MR (**f**, yellow arrow) images

all the other 958 originally extracted ones. Furthermore, value distribution of both GLV and HGLZE are significantly different between LN-positive and LN-negative patients ($p < 0.005$). A scatterplot of GLV and HGLZE values with respect to the presence/absence of LN involvement is shown in Fig. 5.

Finally, according to ROC analyses, the two original GLSZM features resulted good predictors of LN involvement, both with an AUC of 0.992 (95% CI: 0.95–1.00) and an optimal cut-off value of 0.145 for GLV (correspondent sensitivity and specificity of 90% and 100%, respectively; Fig. 6a) and of 1.545 for HGLZE (correspondent sensitivity and specificity of 90% and 100%, respectively; Fig. 6b).

Discussion

Radical surgery represents the first-line treatment for resectable PanNETs and specific pathological factors correlate with the risk of recurrence after surgery, therefore having an impact on patients' follow-up and survival [25–27]. The presence of LN metastases is one of the most relevant predictors of recurrence and it is currently preoperatively estimated by assessing tumour grade and radiological diameter [28].

In the present study, the role of fully hybrid ^{68}Ga-DOTATOC PET/MRI-derived parameters in predicting LN involvement has been shown. Precisely, both SUVmax and SUVmean showed predictive power, even though correlations' statistical significance was lost after correcting for multiple testing, likely because of the cohort size. Moreover, two original GLSZM texture features extracted from T2 MRI sequences (GrayLevelVariance and HighGrayLevelZoneEmphasis) resulted good predictors of LN involvement as well, also demonstrating significant correlations.

So far, few studies have investigated the predictive value of imaging on PanNET histopathological prognostic factors, considering both PET and MR as imaging techniques [21]. The innovation of the present study relies on the evaluation of both PET and MRI quantitative parameters and radiomic features, investigating their predictive role on histopathological characteristics, in a selective and homogeneous cohort of patients affected by PanNETs and studied with a simultaneous ^{68}Ga-DOTATOC PET/MRI scan prior surgery.

One study only, performed by Bruckmann et al., investigated the role of ^{68}Ga-DOTATOC PET/MRI-derived parameters in a cohort of 26 patients with therapy-naive NENs, showing a significant negative correlation between arterial enhancement and tumour grading [21]. Even though a significant p value was not observed in the present study, agreement was established between the 95% CIs. Moreover, Bruckmann et al. also showed significant associations between tumour aggressiveness and arterial phase hyperenhancement, and diffusion restriction and SUVmax above the hepatic level were observed [21]. Interestingly, a significant correlation between SUVmax and tumour's grade was also observed in another study performed on 38 NEN patients, studied with PET/CT [29]. To the best of our knowledge, the

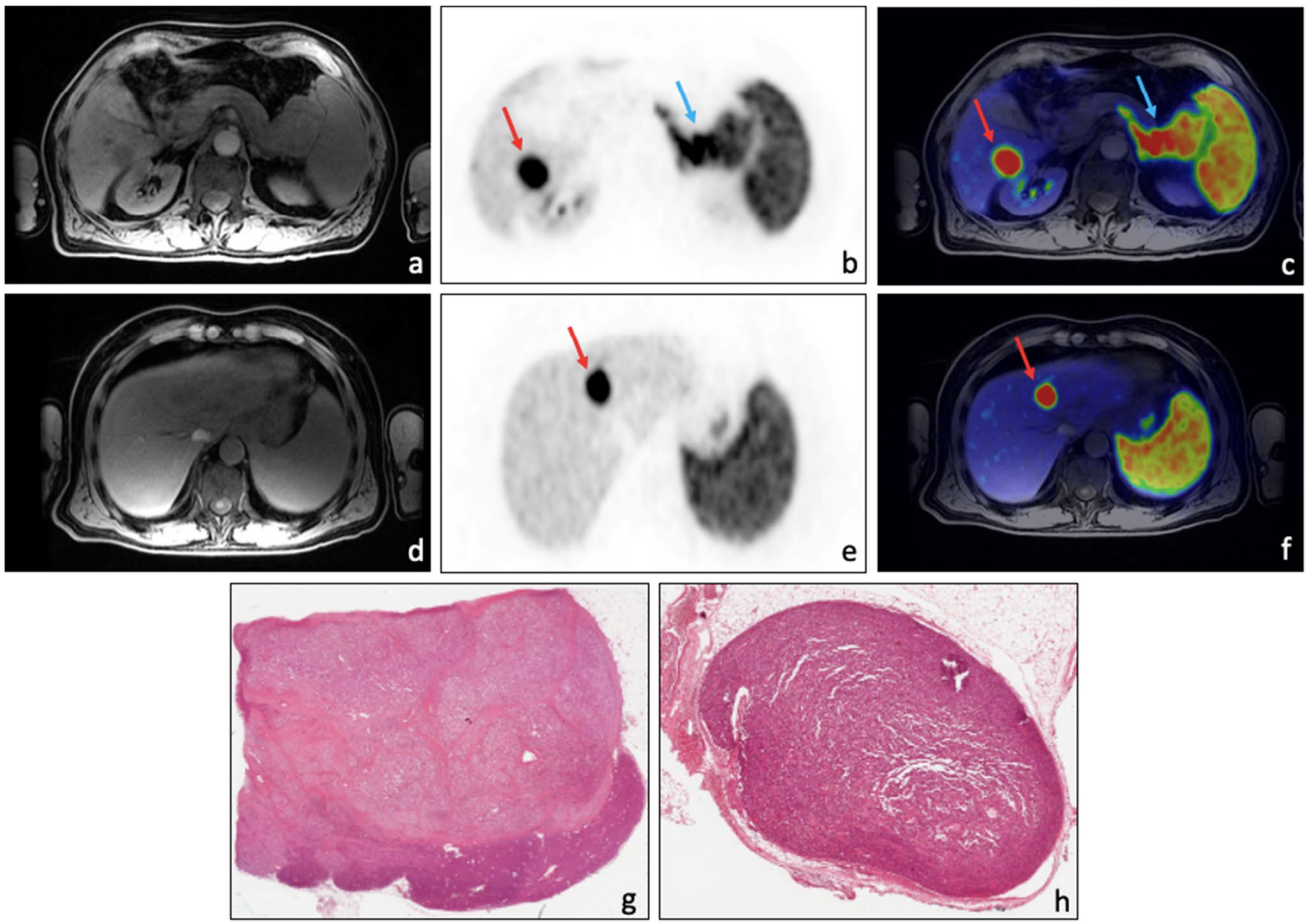

Fig. 3 ^{68}Ga-DOTATOC PET/MRI performed for PanNET staging. A 60-year-old patient underwent ^{68}Ga-DOTATOC PET/MRI. ^{68}Ga-DOTATOC PET/MRI showed intense uptake in correspondence of the pancreatic tail (**a**: axial Lava Flex MRI; **b**: axial ^{68}Ga-DOTATOC PET, cyan blue arrow; **c**: axial ^{68}Ga-DOTATOC PET/MRI, cyan blue arrow) and two pathological uptakes in correspondence of the VI (**b** and **c**: red arrow) and IV hepatic segments (**d**: axial Lava Flex MRI; **e**: axial ^{68}Ga-DOTATOC PET, red arrow; **f**: axial ^{68}Ga-DOTATOC PET/MRI, red arrow); **g**: histological section, haematoxylin and eosin stain of the primary PanNET (G2; Ki67: 5%); **h**: histological section, haematoxylin and eosin stain of a lymph node entirely replaced by the tumour

present study represents the first investigation on the role of ^{68}Ga-DOTATOC PET/MRI-derived parameters in the field of PanNETs, as we specifically included only patients with PanNET, and not NEN arising from other sites. Additionally, the gold standard for our analysis was the histological examination, as all patients underwent surgery, while in the study conducted by Bruckmann and colleagues, a number of patients had only biopsy as reference standard and this aspect might have hampered and biased the statistical power of the analysis.

Another relevant aspect of our investigation is the exploration of the potentiality of radiomic features extracted from both PET and MRI in predicting specific histopathological features of PanNET aggressiveness. Precisely, we demonstrated an inverse correlation between the two original GLSZM texture features extracted from T2 MRI sequences and lymphnodal involvement. Specifically, HGLVE measures the distribution of higher gray level values, with a higher value indicating a greater proportion of higher gray level values and size zones in the image, while GLV measures the variance in gray level intensities for the zones. Given their definition and their belonging to the class of texture features, these parameters provide a representation of the heterogeneity among the pixels within a specific image, which in turn reflects the heterogeneity of tumour's pathophysiological tissues. The meaning of the inverse correlation that we found between GLSZM features and LN involvement is that lower features' values correspond to a smaller homogeneity of gray values within the image, and therefore to a higher tumour's heterogeneity. This, in turn, brings to a higher probability to have lymphnodal involvement [30, 31]. Tumour heterogeneity represents a critical issue, especially in PanNETs, where fine-needle aspiration biopsy might not be fully representative of this aspect of the

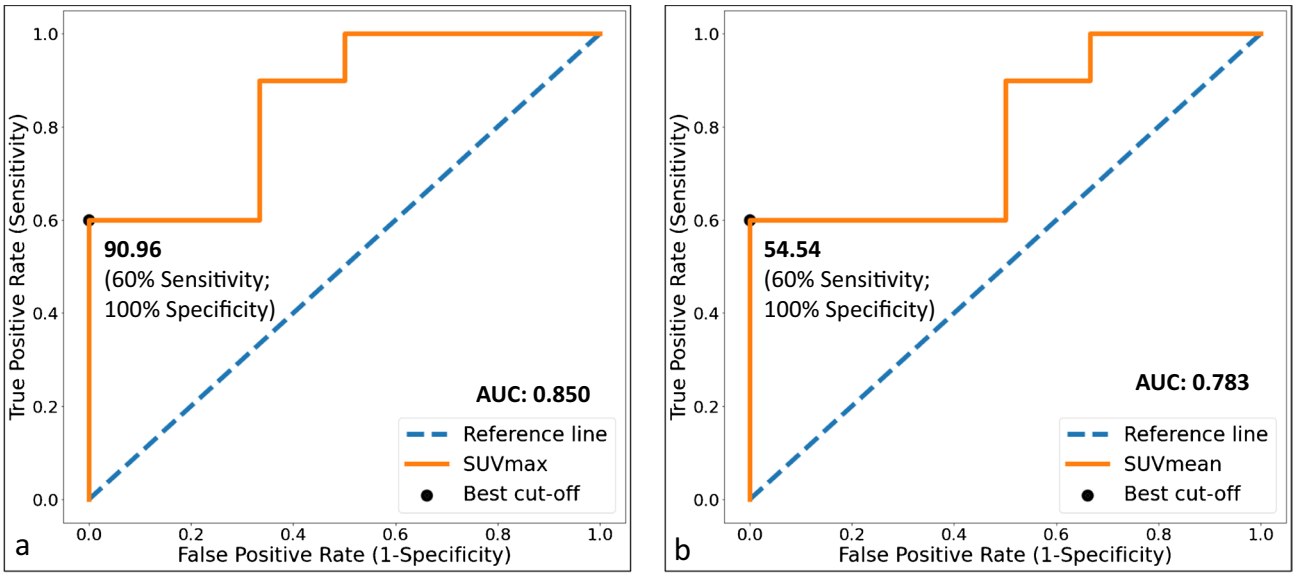

Fig. 4 ROC curves of PET-derived SUVmax (**a**) and SUVmean (**b**) parameters as predictors of lymphnodal involvement. Dotted blue lines represent an area under the curve (AUC) equal to 0.5 (i.e., random condition), while solid orange lines represent the AUCs obtained for the SUVmax (**a**) and SUVmean (**b**) parameters, respectively. Black points represent optimal cut-offs, with a value of 90.96 (correspondent sensitivity and specificity of 60% and 100%, respectively) for SUVmax, and 54.54 (correspondent sensitivity and specificity of 60% and 100%, respectively) for SUVmean

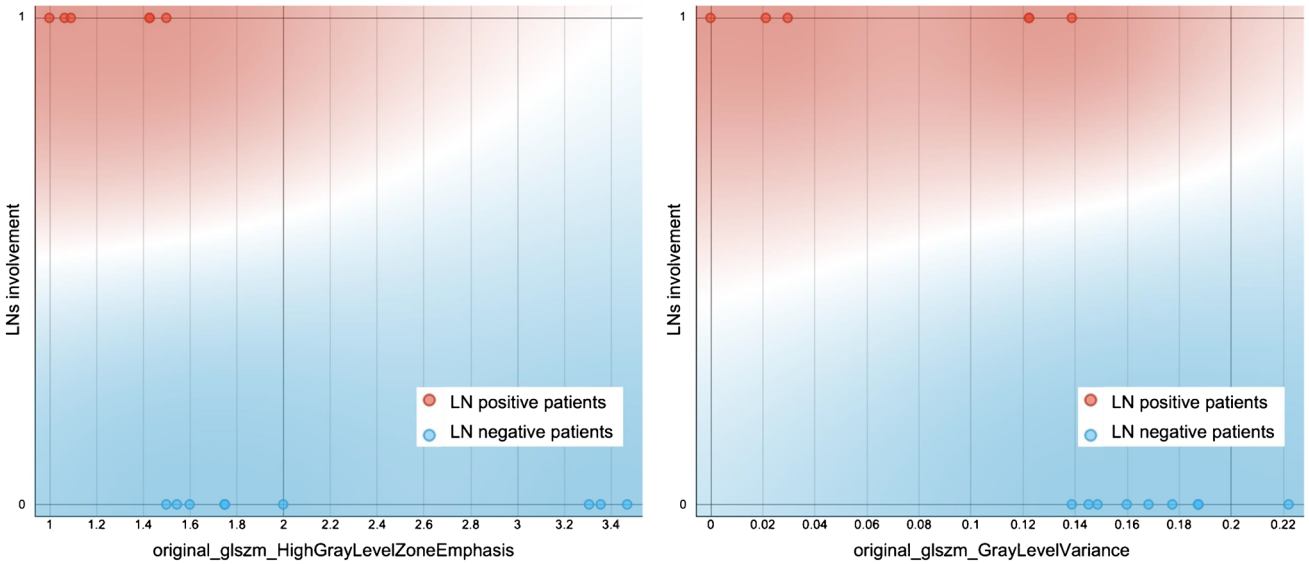

Fig. 5 Scatterplots of GLV and HGLZE with respect to lymphnodal involvement. The two original gray level size zone matrix (GLSZM) texture features GrayLevelVariance (GLV) and HighGrayLevelZoneEmphasis (HGLZE) were extracted from T2 MRI sequences. LN-positive patients and LN-negative patients, as defined by histopathological analysis, are shown in red and light-blue colour, respectively. On the *y*-axis, 0 represents the LN-negative class, while 1 represents the LN-positive class

tumour. Additionally, tumour heterogeneity is not such easily detectable by qualitative analysis of molecular and morphological imaging. In this scenario, the power of radiomics relies in the ability to detect useful, non-visible insights which may depict possible tumour features of aggressiveness [32]. Notably, this could be the reason why, in our study, texture features resulted to be more robust compared to quantitative PET/MRI parameters. In fact, considering the lower number of patients, texture features showed higher values of correlation, whose statistical significance held true also after adjustment for multiple testing, compared to quantitative parameters. Precisely, the correction for multiple

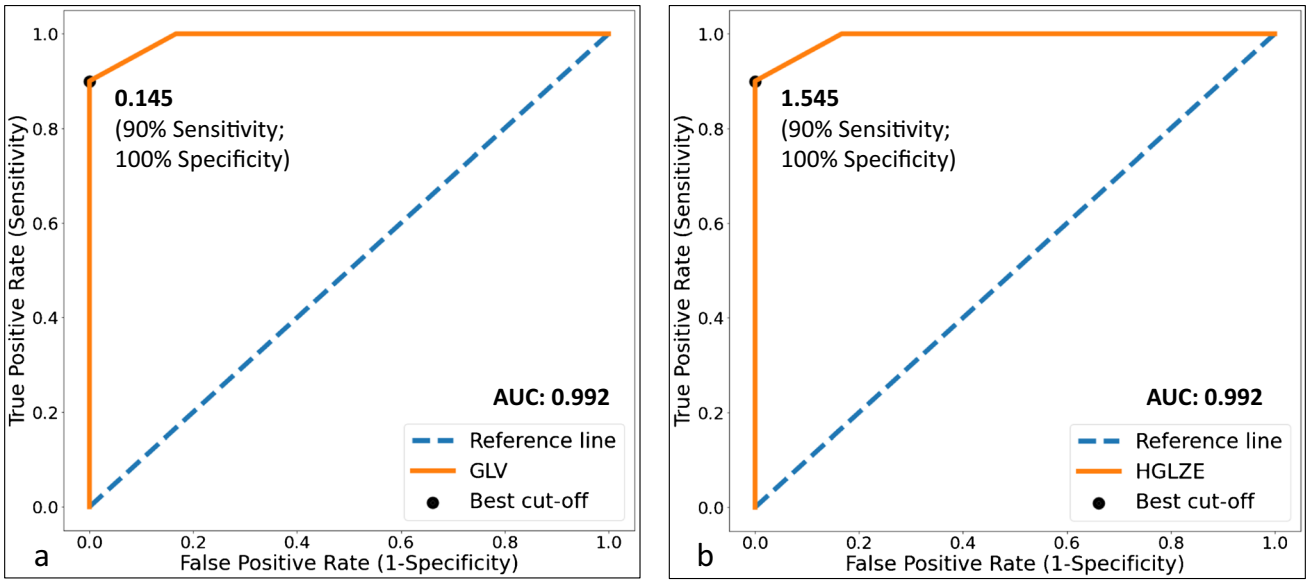

Fig. 6 ROC curves of MRI-derived GLV (**a**) and HGLZE (**b**) radiomic features as predictors of lymphnodal involvement. The two original gray level size zone matrix (GLSZM) texture features GrayLevelVariance (GLV) and HighGrayLevelZoneEmphasis (HGLZE) were extracted from T2 MRI sequences. Dotted blue lines represent an area under the curve (AUC) equal to 0.5 (i.e., random condition), while solid orange lines represent the AUCs obtained for GLV (**a**) and HGLZE (**b**), respectively. Black points represent optimal cut-offs, with a value of 0.145 (correspondent sensitivity and specificity of 90% and 100%, respectively) for GLV, and 1.545 (correspondent sensitivity and specificity of 90% and 100%, respectively) for HGLZE

testing was performed for taking into account a statistical confidence measure that was comprehensive of all investigation performed for each parameter, on both imaging and radiomic features [33]. In fact, when a single parameter is tested, a *p* value lower than 0.05 indicates that there is less than a 5% probability that the results are random. By testing different parameters, however, this probability increases, and *p* values associated to each of the imaging and radiomic parameters had to be adjusted, resulting in the loss of significance for SUVmax and SUVmean imaging parameters, while corroborating the correlations of GLV and HGLVE radiomic features.

The application of the radiomic approach to PET/MR scans for the evaluation of PanNET prognostic factors and aggressiveness has not been previously investigated. Only one study, performed by Weber et al., evaluated the differences between peptide receptor radionuclide therapy (PRRT)-responders and non-responders by comparing the differences in PET- and ADC maps–derived imaging and radiomic parameters extracted from ^{68}Ga-DOTATOC-PET/MRI performed before treatment [19]. They observed that responders showed a borderline significant decrease in entropy on ADC maps, compared to non-responders, even though no parameters were able to predict treatment response to PRRT on pre-therapeutic ^{68}Ga-DOTATOC-PET/MRI, probably because of the small sample size.

Differently, few studies investigated the application of radiomics on either PET or MR scans separately [6, 17, 34, 35]. Bevilacqua and colleagues [17] explored the ability of radiomic features extracted from ^{68}Ga-DOTANOC PET/CT in predicting tumour grading, while Mapelli et al. investigated the role of texture features derived from ^{68}Ga-DOTATOC and 18F-FDG PET/CT in predicting PanNET diameter, angioinvasion, and lymphnodal involvement [6]. De Robertis and colleagues [34] evaluated instead MRI-derived radiomic features in predicting tumour grade, vascular involvement, and lymphnodal and liver metastases in PanNETs, while Bian et al. used texture features derived from non-contrast MRI images to provide a good preoperative discrimination between G1 and G2-G3 PanNETs [35].

One of the main limitations that could be pointed out for our study is the limited number of recruited patients. However, it has to be noted that PanNETs are very rare tumours and the primary staging is still only occasionally performed on PET/MRI scanners. Moreover, differently from similar and previous published studies [21, 36, 37], our cohort of patients is homogeneous in terms of site of origin of primary NEN (all pancreatic) and histological examination was the gold standard in all patients. Finally, it has to be reminded that patients involved in this work are part of a larger prospective study, and performed analyses and obtained results will be further validated on more comprehensive cohorts, along with advanced investigations on the possible role and synergy of ^{68}Ga-DOTATOC PET/MRI and radiomic parameters

in assessing PanNETs' histopathological prognostic factors. This will also allow to evaluate the robustness of ROC curves' cut-off values found in the present work. Despite being very informative, cut-off values identified through ROC curves are indeed difficult to reproduce in different cohorts of patients, especially if the thresholds have been identified in a small cohort for patients as the one presented, and further analyses will allow to assess results' reproducibility.

Acknowledgements The SIGNA PET/MRI system (General Electric Healthcare, Waukesha, WI, USA) used in the present work has been purchased with funding from the Italian Ministry of Health.

Declarations

Ethical approval. All procedures performed in studies involving human participants were in accordance with the ethical standards of the institutional and national research committee and with the 1964 Helsinki Declaration and its later amendments or comparable ethical standards.

Consent to participate All patients gave their informed consent to participate to the study.

Conflict of interest Prof. Massimo Falconi is Advisory Board Member of Advanced Accelerator Application (AAA). All the other authors have no conflicts of interest related to the present paper to disclose.

References

1. Klimstra DS, Beltran H, Lilenbaum R, Bergsland E. The spectrum of neuroendocrine tumors: histologic classification, unique features and areas of overlap. Am Soc Clin Oncol Educ Book. 2015:92–103. https://doi.org/10.14694/EdBook_AM.2015.35.92.
2. Sun J. Pancreatic neuroendocrine tumors. Intractable Rare Dis Res. 2017;6:21–8. https://doi.org/10.5582/irdr.2017.01007.
3. Bozkurt MF, Virgolini I, Balogova S, Beheshti M, Rubello D, Decristoforo C, et al. Guideline for PET/CT imaging of neuroendocrine neoplasms with (68)Ga-DOTA-conjugated somatostatin receptor targeting peptides and (18)F-DOPA. Eur J Nucl Med Mol Imaging. 2017;44:1588–601. https://doi.org/10.1007/s00259-017-3728-y.
4. Ambrosini V, Campana D, Polverari G, Peterle C, Diodato S, Ricci C, et al. Prognostic value of 68Ga-DOTANOC PET/CT SUVmax in patients with neuroendocrine tumors of the pancreas. J Nucl Med. 2015;56:1843–8. https://doi.org/10.2967/jnumed.115.162719.
5. Mapelli P, Partelli S, Salgarello M, Doraku J, Muffatti F, Schiavo Lena M, et al. Dual tracer 68Ga-DOTATOC and 18F-FDG PET improve preoperative evaluation of aggressiveness in resectable pancreatic neuroendocrine neoplasms. Diagnostics (Basel). 2021;11. https://doi.org/10.3390/diagnostics11020192.
6. Mapelli P, Partelli S, Salgarello M, Doraku J, Pasetto S, Rancoita PMV, et al. Dual tracer 68Ga-DOTATOC and 18F-FDG PET/computed tomography radiomics in pancreatic neuroendocrine neoplasms: an endearing tool for preoperative risk assessment. Nucl Med Commun. 2020;41:896–905. https://doi.org/10.1097/MNM.0000000000001236.
7. Pichler BJ, Wehrl HF, Kolb A, Judenhofer MS. Positron emission tomography/magnetic resonance imaging: the next generation of multimodality imaging? Semin Nucl Med. 2008;38:199–208. https://doi.org/10.1053/j.semnuclmed.2008.02.001.
8. Hofman MS, Lau WF, Hicks RJ. Somatostatin receptor imaging with 68Ga DOTATATE PET/CT: clinical utility, normal patterns, pearls, and pitfalls in interpretation. Radiographics. 2015;35:500–16. https://doi.org/10.1148/rg.352140164.
9. Hope TA, Pampaloni MH, Nakakura E, VanBrocklin H, Slater J, Jivan S, et al. Simultaneous (68)Ga-DOTA-TOC PET/MRI with gadoxetate disodium in patients with neuroendocrine tumor. Abdom Imaging. 2015;40:1432–40. https://doi.org/10.1007/s00261-015-0409-9.
10. Mapelli P, De Cobelli, F, Picchio M. PET/MRI in neuroendocrine tumours: blessings and curses. Current Radiopharmaceuticals. 2019;12.
11. Mapelli P, Ironi G, Fallanca F, Partelli S, Muffatti F, Andreasi V, Gianolli L, Falconi M, De Cobelli F, Picchio M. 68Ga-DOTA-peptides PET/MRI in pancreatico-duodenal neuroendocrine tumours: a flash pictorial essay on assets and lacks. Clin Transl Imaging. 2019;7:363–71.
12. Humphrey PE, Alessandrino F, Bellizzi AM, Mortele KJ. Non-hyperfunctioning pancreatic endocrine tumors: multimodality imaging features with histopathological correlation. Abdom Imaging. 2015;40:2398–410. https://doi.org/10.1007/s00261-015-0458-0.
13. Oksuz MO, Winter L, Pfannenberg C, Reischl G, Mussig K, Bares R, et al. Peptide receptor radionuclide therapy of neuroendocrine tumors with (90)Y-DOTATOC: is treatment response predictable by pre-therapeutic uptake of (68)Ga-DOTATOC? Diagn Interv Imaging. 2014;95:289–300. https://doi.org/10.1016/j.diii.2013.07.006.
14. Rha SE, Jung SE, Lee KH, Ku YM, Byun JY, Lee JM. CT and MR imaging findings of endocrine tumor of the pancreas according to WHO classification. Eur J Radiol. 2007;62:371–7. https://doi.org/10.1016/j.ejrad.2007.02.036.
15. Mayerhoefer ME, Materka A, Langs G, Haggstrom I, Szczypinski P, Gibbs P, et al. Introduction to radiomics. J Nucl Med. 2020;61:488–95. https://doi.org/10.2967/jnumed.118.222893.
16. Bezzi C, Mapelli P, Presotto L, Neri I, Scifo P, Savi A, et al. Radiomics in pancreatic neuroendocrine tumors: methodological issues and clinical significance. Eur J Nucl Med Mol Imaging. 2021. https://doi.org/10.1007/s00259-021-05338-8
17. Bevilacqua A, Calabro D, Malavasi S, Ricci C, Casadei R, Campana D, et al. A [68Ga]Ga-DOTANOC PET/CT radiomic model for non-invasive prediction of tumour grade in pancreatic neuroendocrine tumours. Diagnostics (Basel). 2021;11. https://doi.org/10.3390/diagnostics11050870.
18. Onner H, Abdulrezzak U, Tutus A. Could the skewness and kurtosis texture parameters of lesions obtained from pretreatment Ga-68 DOTA-TATE PET/CT images predict receptor radionuclide therapy response in patients with gastroenteropancreatic neuroendocrine tumors? Nucl Med Commun. 2020;41:1034–9. https://doi.org/10.1097/MNM.0000000000001231.
19. Weber M, Kessler L, Schaarschmidt B, Fendler WP, Lahner H, Antoch G, et al. Treatment-related changes in neuroendocrine tumors as assessed by textural features derived from (68)Ga-DOTATOC PET/MRI with simultaneous acquisition of apparent diffusion coefficient. BMC Cancer. 2020;20:326. https://doi.org/10.1186/s12885-020-06836-y.
20. Werner RA, Ilhan H, Lehner S, Papp L, Zsoter N, Schatka I, et al. Pre-therapy somatostatin receptor-based heterogeneity predicts overall survival in pancreatic neuroendocrine tumor patients undergoing peptide receptor radionuclide therapy. Mol Imaging Biol. 2019;21:582–90. https://doi.org/10.1007/s11307-018-1252-5.
21. Bruckmann NM, Rischpler C, Kirchner J, Umutlu L, Herrmann K, Ingenwerth M, et al. Correlation between contrast

enhancement, standardized uptake value (SUV), and diffusion restriction (ADC) with tumor grading in patients with therapy-naive neuroendocrine neoplasms using hybrid (68)Ga-DOTA-TOC PET/MRI. Eur J Radiol. 2021;137:109588. https://doi.org/10.1016/j.ejrad.2021.109588.
22. Taha AA, Hanbury A. Metrics for evaluating 3D medical image segmentation: analysis, selection, and tool. BMC Med Imaging. 2015;15:29. https://doi.org/10.1186/s12880-015-0068-x.
23. Klimstra DS, Kloppell G, La Rosa S and Rindi G. Digestive system tumours. WHO classification of tumours 2019;1. IARC, Lyon.
24. Koo TK, Li MY. A guideline of selecting and reporting intraclass correlation coefficients for reliability research. J Chiropr Med. 2016;15:155–63. https://doi.org/10.1016/j.jcm.2016.02.012.
25. Curran T, Pockaj BA, Gray RJ, Halfdanarson TR, Wasif N. Importance of lymph node involvement in pancreatic neuroendocrine tumors: impact on survival and implications for surgical resection. J Gastrointest Surg. 2015;19:152–60; discussion 60. https://doi.org/10.1007/s11605-014-2624-z.
26. Ellison TA, Wolfgang CL, Shi C, Cameron JL, Murakami P, Mun LJ, et al. A single institution's 26-year experience with nonfunctional pancreatic neuroendocrine tumors: a validation of current staging systems and a new prognostic nomogram. Ann Surg. 2014;259:204–12. https://doi.org/10.1097/SLA.0b013e31828f3174.
27. Falconi M, Eriksson B, Kaltsas G, Bartsch DK, Capdevila J, Caplin M, et al. ENETS consensus guidelines update for the management of patients with functional pancreatic neuroendocrine tumors and non-functional pancreatic neuroendocrine tumors. Neuroendocrinology. 2016;103:153–71. https://doi.org/10.1159/000443171.
28. Partelli S, Javed AA, Andreasi V, He J, Muffatti F, Weiss MJ, et al. The number of positive nodes accurately predicts recurrence after pancreaticoduodenectomy for nonfunctioning neuroendocrine neoplasms. Eur J Surg Oncol. 2018;44:778–83. https://doi.org/10.1016/j.ejso.2018.03.005.
29. Kayani I, Bomanji JB, Groves A, Conway G, Gacinovic S, Win T, et al. Functional imaging of neuroendocrine tumors with combined PET/CT using 68Ga-DOTATATE (DOTA-DPhe1, Tyr3-octreotate) and 18F-FDG. Cancer. 2008;112:2447–55. https://doi.org/10.1002/cncr.23469.
30. Caswell DR, Swanton C. The role of tumour heterogeneity and clonal cooperativity in metastasis, immune evasion and clinical outcome. BMC Med. 2017;15:133. https://doi.org/10.1186/s12916-017-0900-y.
31. Stanta G, Bonin S. Overview on clinical relevance of intra-tumor heterogeneity. Front Med (Lausanne). 2018;5:85. https://doi.org/10.3389/fmed.2018.00085.
32. Zwanenburg A, Vallieres M, Abdalah MA, Aerts H, Andrearczyk V, Apte A, et al. The image biomarker standardization initiative: standardized quantitative radiomics for high-throughput image-based phenotyping. Radiology. 2020;295:328–38. https://doi.org/10.1148/radiol.2020191145.
33. Noble WS. How does multiple testing correction work? Nat Biotechnol. 2009;27:1135–7. https://doi.org/10.1038/nbt1209-1135.
34. De Robertis R, Maris B, Cardobi N, Tinazzi Martini P, Gobbo S, Capelli P, et al. Can histogram analysis of MR images predict aggressiveness in pancreatic neuroendocrine tumors? Eur Radiol. 2018;28:2582–91. https://doi.org/10.1007/s00330-017-5236-7.
35. Bian Y, Zhao Z, Jiang H, Fang X, Li J, Cao K, et al. Noncontrast radiomics approach for predicting grades of nonfunctional pancreatic neuroendocrine tumors. J Magn Reson Imaging. 2020;52:1124–36. https://doi.org/10.1002/jmri.27176.
36. Abdulrezzak U, Kurt YK, Kula M, Tutus A. Combined imaging with 68Ga-DOTA-TATE and 18F-FDG PET/CT on the basis of volumetric parameters in neuroendocrine tumors. Nucl Med Commun. 2016;37:874–81. https://doi.org/10.1097/MNM.0000000000000522.
37. Campana D, Ambrosini V, Pezzilli R, Fanti S, Labate AM, Santini D, et al. Standardized uptake values of (68)Ga-DOTANOC PET: a promising prognostic tool in neuroendocrine tumors. J Nucl Med. 2010;51:353–9. https://doi.org/10.2967/jnumed.109.066662.